J. Sens. Sens. Syst., 5, 197–203, 2016
www.j-sens-sens-syst.net/5/197/2016/
doi:10.5194/jsss-5-197-2016

JSSS Journal of Sensors and Sensor Systems Open Access

Offset stable piezoresistive high-temperature pressure sensors based on silicon

Robert Täschner, Erik Hiller, and Michael Blech

CiS Forschungsinstitut für Mikrosensorik GmbH, 99099 Erfurt, Germany

Correspondence to: Robert Täschner (rtaeschner@cismst.de)

Received: 24 February 2016 – Revised: 17 May 2016 – Accepted: 18 May 2016 – Published: 8 June 2016

Abstract. The exploitation of new application fields and the drive to size reduction even in highly stable pressure sensing systems makes the extension of the operating temperature range of the microelectromechanical sensors (MEMS) essential. For this reason a silicon-based pressure sensor with an application temperature ranging up to 300 °C and the associated manufacturing technology was developed. With special design and manufacturing approaches mounting stress-insensitive sensors with high linearity, excellent offset stability, low hysteresis and low sensitivity changes over the entire temperature range were developed. At the moment, the sensors are tested till 300 °C at wafer level and between 135 and 210 °C as a first-level package.

1 Introduction

The pressure is one of the main values for the industrial process and control technology. Nearly every piece of complex processing equipment is equipped with at least one pressure sensing element which can also be seen in the sales volume of around 1×10^9 microelectromechanical pressure sensors (MEMS) in 2015 (Yole Développement, 2015). In recent years, there has been a tendency for miniaturisation even in high-precision applications that cannot be resolved by a further reduction of the dimensions of the MEMS sensing element (Wohlgemuth, 2008). New possibilities for smaller, better and cheaper measurement cells have to be achieved by an enhancement of the sensor functions like an extension of the operation temperature. The goal of our research was to develop a silicon-based piezoresistive pressure sensor that delivers a full measurement capability up to 300 °C without a loss of sensor performance in the standard temperature range. With such a sensing element it is possible to build smaller measurement systems with improved dynamics, better overall performance and economical benefits.

2 Process development of the silicon-on-insulator technology

One of the main challenges in the realisation of a high-temperature silicon pressure sensor is the thermal generated leakage current. These leakage currents are the main drawback of conventional sensors that are using a p–n junction as isolation between the sensing elements and the silicon substrate as they rise from room temperature to 300 °C by about 5 orders of magnitude (Soler and Galo, 2009). One possibility to overcome this problem is the usage of silicon-on-insulator (SOI) techniques and the complete dielectric insulation of the sensing elements. Silicon layer thickness of 1–5 µm are of special interest for this application. Unfortunately, this thickness region is difficult to process with conventional SOI techniques. The use of ion implantation-based techniques like SMARTCUT or separation by implanted oxygen (SIMOX) will require extremely high implantation energies, which can be easily re-enacted, for example with simulation tools, combined with high doses (Celler and Cristoloveanu, 2003).

On the other hand, if back-etch or grind techniques are used there is a significant influence of the etching homogeneity and the total thickness variation (TTV) of the device or handle wafer, respectively, as the reference surface within the process is not the later surface of the device layer.

To overcome these problems for the fabrication of the high-temperature pressure sensors we developed an SOI technique based on an existing etching approach (Wang et al., 1992). In contrast to the mainly used electrochemical etch stop (that uses a constant potential and an n-type stop layer that leads to a stop at or shortly before the reverse biased p–n transition because of the rising current and the involved shift in the potential) we used a pulsed etching technique. This technology makes use of the differing electrochemical properties of the layers. The electrochemical oxidation rate of p-type silicon in the unilluminated case is significantly higher than the oxidation rate of n-type silicon as the process is driven by the holes. This can be used to realise an etch stop without the drawbacks of the unpulsed alternative that suffers from possible defects in the large diode region or the uneven stop on the p–n transition (Soßna, 2002). Both effects can lead to a premature passivation of the silicon that should be etched before the p–n transition is reached completely.

For the identification of a possible process window we evaluated the passivation times. They were defined as the times to reach 80 % of the electrochemical potential after a current pulse. Aqueous potassium hydroxide solutions with a fixed pulse length of 2 s and varying potentials in combination with p-type wafers with a bulk resistivity of 10–20 Ω × cm and n-type wafers with a bulk resistivity of 3–5 Ω × cm were used.

It can be recognised in Fig. 1 that a significant variation in the passivation time can be achieved by a conductivity type change. This significant change can be explained by the high quantity of majority carriers (holes) in the p-type material. Based on the difference in the oxidation rates we decided to start a test of SOI technology. n-type wafers were boron implanted and annealed. These wafers are bonded against oxidised p-type carrier wafers that had the oxide striped at the 7 mm edge. The silicon fusion bonding (SFB) process assures an electrical contact to the p-type region of the device wafer at the wafer edge and, at the same time, a dielectric insulation at the wafer core. After a conventional pre-etching step in 30 m % KOH (aq) at 80 °C we used pulsed electrochemical etching at 60 °C to realise an etch stop at the p-type region of the device wafer.

It can be seen from Fig. 2 that by using the given parameters it is possible to achieve an etch rate of 0.2 µm × min^{-1} within the n-type region. As soon as the p-type region is reached there is no direct attack of the silicon as the mean buildup rate of the SiO_2 is higher than the mean etch rate of SiO_2 in 30 m % KOH (aq) at 60 °C. As a consequence of this fact the etch rate is lowered to < 2 nm × min^{-1}. Starting with a TTV of over 10 µm this SOI technique makes it possible to form device layers with a deviation of less than 200 nm over the entire core diameter of a wafer which can be further reduced by process improvement. Furthermore, there is no tendency for a premature passivation of the n-type region even if there are defects in the doping area.

3 Silicon fusion bonding

Silicon pressure sensor packages aiming for a wide temperature sensor range have to be assembled via silicon fusion bonding. Heterogeneous material combinations with differing coefficients of thermal expansion lead to very high thermal-induced stress levels within the package and are therefore (in principle) unsuited. To guarantee good process compatibility we used low-temperature silicon direct bonding with annealing temperatures lower than 400 °C. The new sensor should be usable as a differential pressure sensor which means that both sides of the sensor could be exposed to the process pressure and as a gauge pressure sensor system where only one side is exposed to the process pressure and the other side is referenced to the ambient pressure. That means that there is a need for the evaluation of the fracture toughness of the SFB interface under the influence of temperature changes, silicone oils for the application of a differential pressure sensor and humidity for the application as a gauge pressure sensor. For the measurement of the interface fracture toughness we used micro-chevron (mc) structures (Bring, 2006). As activations for the SFB process pre-optimized RF plasma, DC-biased RF plasma and DC plasma processes were executed. These processes assure a sufficient toughness for the sensor at an annealing temperature of 325 °C. The temperature stress test was performed between −50 and 150 °C for 100 cycles. None of the plasma-

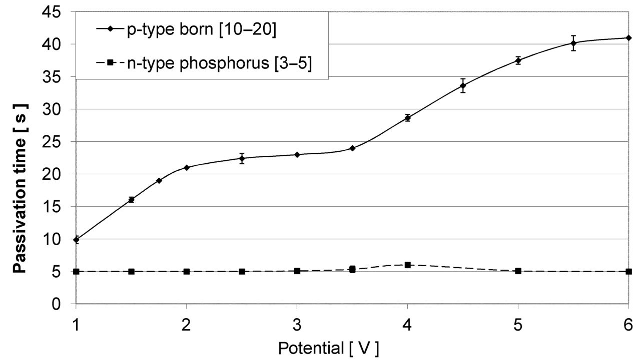

Figure 1. Conductivity type and potential-dependent passivation time at 2 s pulse length.

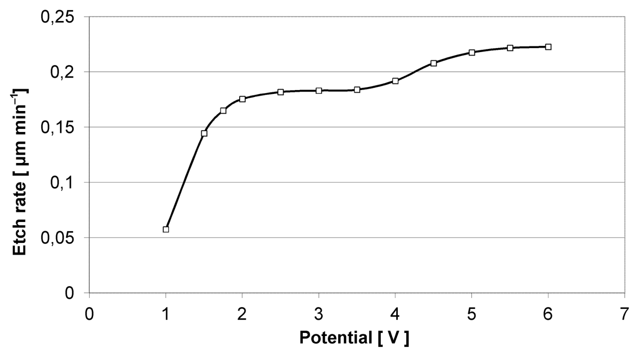

Figure 2. Potential-dependent etch rate at 2 s pulse time in 30 m % KOH (aq) at 60 °C.

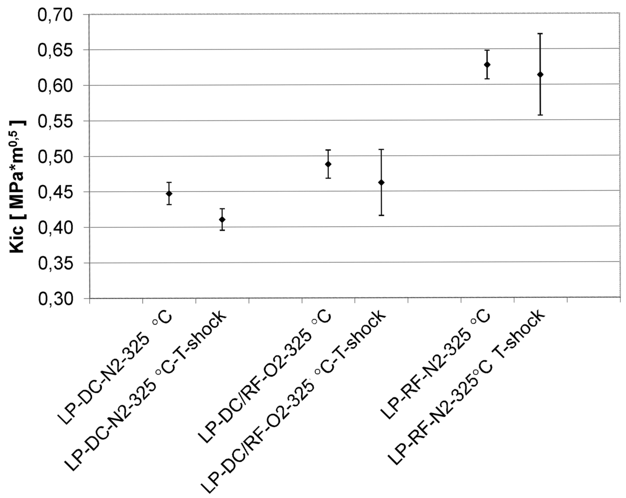

Figure 3. Fracture toughness before and after 100 temperature cycles between −50 and 150 °C.

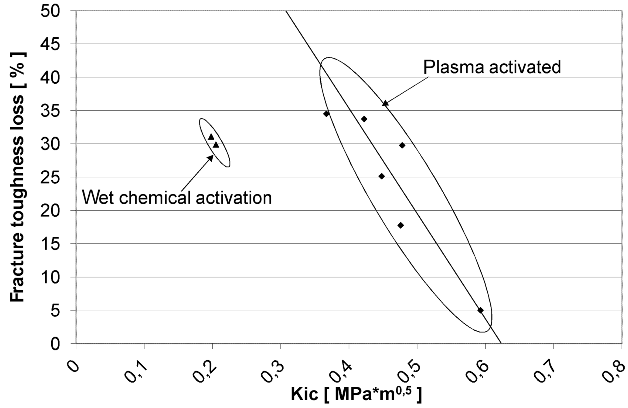

Figure 4. Humidity-dependent loss of fracture toughness.

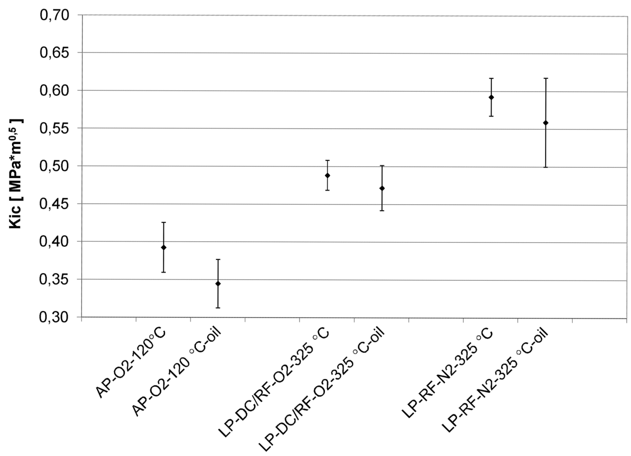

Figure 5. SFB toughness behaviour with and without contact to AK20 silicone oil.

activated samples showed a significant change in fracture toughness after the temperature cycles.

As shown in Fig. 3, there is a slight increase in the spreading of the measurement results after the temperature cycles. This increase is within the normal range of such measurements, a direct interference to the temperature cycles is therefore difficult.

The increase in fracture toughness within the SFB annealing is based on the condensation of silanol groups. This condensation is an equilibrium reaction that could be shifted by mechanical stress (Soler and Galo, 2009; Lechenault et al., 2011).

$$\equiv \mathrm{Si}-\mathrm{OH}+\mathrm{HO}-\mathrm{Si}\equiv\leftrightarrow \mathrm{H_2O}+\equiv\mathrm{Si}-\mathrm{O}-\mathrm{Si}\equiv$$

Particularly, the heavily loaded bonds in front of a fracture that are lengthened but not broken are prone to this equilibrium shift. The opening velocity of the fracture test of the mc samples in direct contact with water was lowered to $1.7\,\mu\mathrm{m}\times\mathrm{s}^{-1}$. This was done to assure the equilibrium between stress-induced corrosion, fracture opening and force time. The formerly described plasma activations with different process parameters and HNO_3 as well as RCA SC1-based wet chemical activations with pre-optimised process parameters were used. Wet chemical activations were also tested, as they provide a very economic alternative for lightly stressed interfaces because of their ability to be done as batch processes.

As shown in Fig. 4 there is a significant influence of the direct contact with water to the fracture toughness and therefore to the stress intensity factor (Kic) that is given in $\mathrm{MPa}\times\mathrm{m}^{-2}$ and describes the resistance against crack propagation of low-temperature SFB interfaces.

It can be seen that the relative loss in fracture toughness is higher for initially weak interfaces than for initially strong interfaces. Fully optimized samples with a fracture toughness as high as $0.6\,\mathrm{MPa}\times\mathrm{m}^{0,5}$ are losing nearly no strength in this test. Figure 4 also indicates that there is a grouping between wet-chemical-activated and plasma-activated samples. We trace this behaviour back to the lower density of plasma oxides compared with wet chemical grown oxides which can be shown by x-ray photoelectron spectroscopy measurements. This could lead to a higher mobility of the humidity within the interface so that it interferes with a higher volume of the loaded structure. SFB packaging of MEMS with potential contact to humidity under load should only be done with optimized plasma activations or high annealing temperatures.

For the test of the resistance against oil under load we decided to use Wacker AK20 since this is a common oil used by the industry for such applications. Figure 5 shows the mean values and the 95 % confidence intervals of the fracture toughness with and without contact to oil.

There is a slight tendency for a reduction of the fracture toughness in contact with silicone oil. In any case the rel-

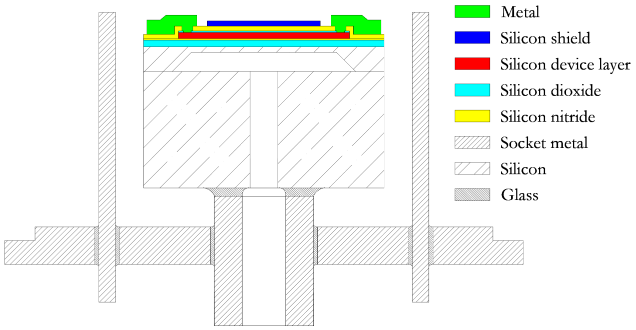

Figure 6. Scheme of the sensor setup.

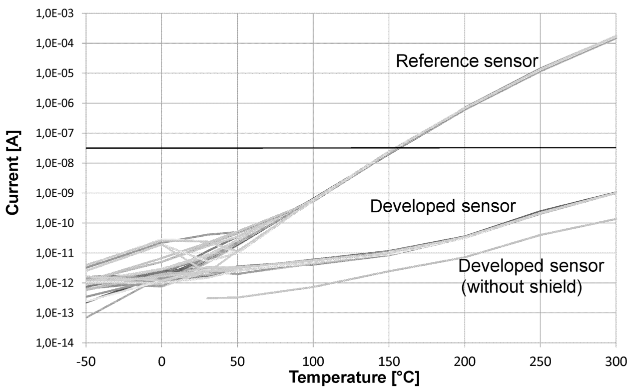

Figure 7. Temperature-dependent leakage currents.

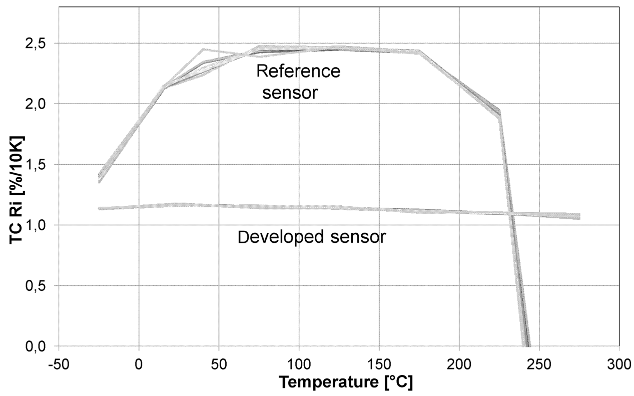

Figure 8. Temperature coefficient of the bridge resistance.

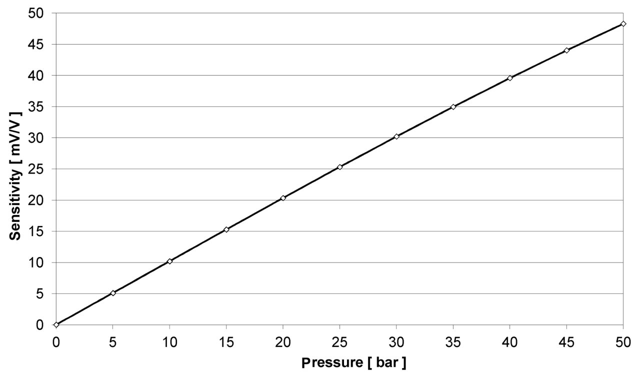

Figure 9. Sensitivity, nominal pressure range is 10 bar.

ative deviation is below 10 % with overlapping confidence intervals. The application of low-temperature SFB interfaces for differential pressure sensors is therefore possible.

4 Sensor design

The pressure sensor was designed for an operating pressure range of 10 bar with a full-scale sensitivity of 2 % for the single-crystalline option and 1 % for the poly-crystalline option. For the single-crystalline option, the conventional approach with the use of the longitudinal and transversal piezoresistive coefficients was used. For the poly-crystalline option, a generalized approach has to be used as the orientation of each crystal varies. Every directorial combination of strain, grain and current must be possible.

$$\pi_l = \pi_{11} + 2(\pi_{44} + \pi_{12} - \pi_{11})(l_1^2 m_1^2 + l_1^2 n_1^2 + m_1^2 n_1^2) \quad (1)$$

$$\pi_t = \pi_{12} - (\pi_{44} + \pi_{12} - \pi_{11})(l_1^2 l_2^2 + m_1^2 m_2^2 + n_1^2 n_2^2) \quad (2)$$

l_1, n_1 and m_1 are the cosines between the longitudinal current flow within the crystal and its crystal axes. l_2, n_2 and m_2 are the cosines between the transversal current flow within the crystal and its crystal axes (Tufte and Stelzer, 1963). The mean components could be acquired by integration of Eqs. (1) and (2) over all possible orientations and weighting by their occurrence (Burns, 1988):

$$\pi_l = \pi_{11} - 0,4(\pi_{11} - \pi_{12} - \pi_{44}) \quad (3)$$

$$\pi_t = \pi_{12} + 0,133(\pi_{11} - \pi_{12} - \pi_{44}). \quad (4)$$

This approach represents an approximation as the real conditions strongly depend on the low pressure chemical vapour deposition conditions. In addition to the orientation dependence, there is a strong relationship between the piezoresistive coefficients and the doping density (Kanda, 1982). For the simulation of the poly-silicon sensor, a doping density of $2.5 \times 10^{19}\,\mathrm{cm}^{-3}$ was chosen. This doping density leads to small temperature cross sensitivities of the sensor and the loss of strain sensitivity is mainly limited to application temperatures 200 °C below what can be extracted from the addressed relationship of the piezo coefficients. In addition, the high doping levels shift the intrinsic region to higher temperatures (Pawlik, 1999), which is also desired.

We focused on three main features in the following sensor design. The first is to achieve a low zero offset, which is a little bit trickier than in a conventional setup, as it is impossible to design symmetric supply conductors with this special resistor layout. This was solved by an optimisation finite element method (FEM) simulation. We started with a cross section as high as possible since the specific conduc-

Figure 10. Characteristic curve deviation.

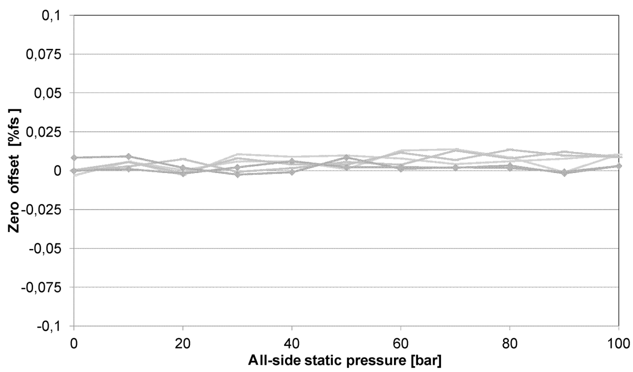

Figure 11. Dependency of the zero offset from static pressures.

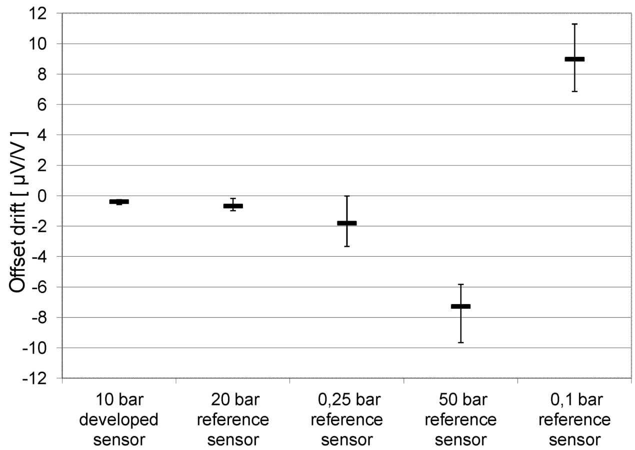

Figure 12. Offset drift over 24 h at 135 °C, anodic bonded sensors.

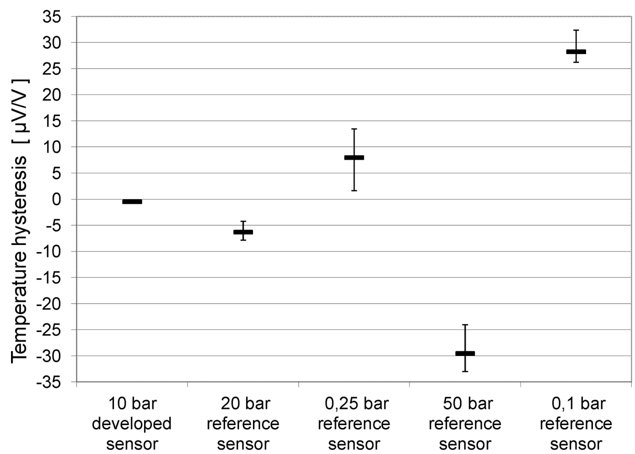

Figure 13. Temperature hysteresis of the zero point after 30/135 °C with 24 h at 135 °C.

tivity spread in poly-silicon that is reachable through doping is smaller than in single-crystalline silicon. The second main feature was a low characteristic curve deviation of the sensor. This parameter could be improved by a compensation of the non-linearity of the signal of the actual sensor elements with the supply conductors. With the supply conductors being strain sensitive it is also possible to position them in such a way that an amount of the non-linearity of the sensor elements is compensated. For this reason the cross section of the supply conductors has to be reduced, which leads to a loss of sensitivity that could be easily compensated by reducing the membrane thickness. The change of the membrane thickness requires a slight repositioning of the sensing elements so that the optimisation has to be done in several iterations. This repeated optimisation ensures the best compromise between sensitivity and non-linearity. The change in stress distribution is not perfectly linear when the pressure on the membrane is altered. This behaviour is different on every point of the membrane. For a small characteristic curve deviation the key is to choose a resistor position where this non-linear component reaches a minimum or, like in our case, if this is not possible because of other compromises, to find a position and dimension of the supply conductors that compensates the non-linearity of the sensor resistors. The stress field under different pressures and its effect on the stress-sensitive parts of the sensor layout can be obtained by coupled FEM simulations. That makes it possible to find combinations of resistors and supply conductors that show nearly no characteristic curve deviation in a specific operation range even when all single elements are showing a non-linear resistivity change. The third main feature that has to be taken into account is the sensitivity to strain within the package. A pressure sensor die with an extremely high operating temperature range especially suffers from mounting stress. Much of the stress that normally occurs when anodic bonding is used as a packaging technique is eliminated by the use of the SFB process. Besides this the interface to the actual measurement system does not end with the 0-level packaging; the sensor has to be mounted on a socket to be used within the system (Fig. 6). In a nominal pressure range of 10 bar hard mounting like the die attach filled with epoxy-based glues must be used to guarantee an adequate pressure stability.

Thermal expansion matched sockets consist, for example, of Kovar (Fe-Ni-Co) with a specific thermal expansion of

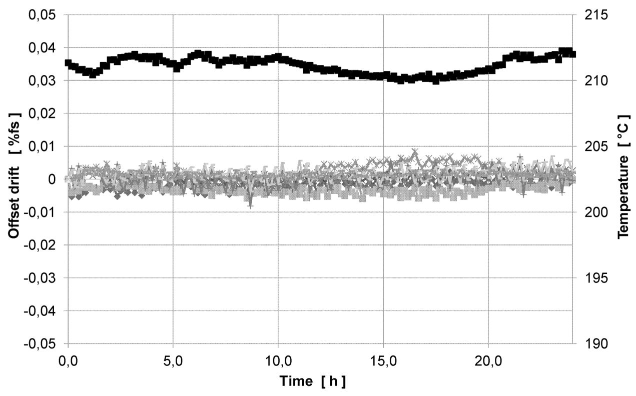

Figure 14. Offset drift at 210 °C.

around 5 ppm. Industrial customers prefer stainless steel as socket material as it offers advantages in the processability and some economical benefits, but its specific thermal expansion is in the range of 10–20 ppm. Silicon has a specific thermal expansion of 2.5–3.8 ppm within the operating temperature range. It can be clearly seen that this material mix must lead to strain within the sensor if it goes through a temperature change. This strain will lead to an offset change and, in particular when plastic materials like epoxy glues are involved, to temperature-dependent drift and hysteresis. Measurements with non-optimised sensors are clearly documenting this behaviour (not shown here).

There is a possibility to separate the two loading conditions, pressure to the membrane and strain within the package. The sensing elements are positioned and optimized via FEM analysis in the way that strain within the package leads to an even load case on all sensing elements and therefore only to a change in the bridge resistance of the sensor. A loading of the membrane by pressure instead will lead to opposite resistance changes in the sensing elements and therefore generates an output signal. This design feature is essential to transmitting the outstanding performance of the MEMS sensors to the completed measurement systems. As this optimisation also leads to shifts in the positions of the sensing elements the other features have to be re-optimised to achieve the best possible compromise for a maximum sensor performance.

5 Evaluation of sensor performance

Firstly, the leakage current was measured over the entire operating temperature range in comparison to a conventional high-performance pressure sensor die that was processed in our own fabrication line as a reference sensor based on junction isolation in the same pressure operating range.

It was possible to reduce the leakage currents at 300 °C by 5–6 orders of magnitude. As shown in Fig. 7, even below 125 °C the developed sensor outperforms the reference sensors clearly. Sensors without an electric shielding show the lowest leakage currents as a leakage path through the Si_3N_4 dielectric to the shield is missing but they are limited in their application as the shielding has to be realised in the higher packaging levels.

The temperature coefficient of the bridge resistance (Fig. 8) of the new sensor is nearly constant over the entire temperature range and shows, in contrast to the reference sensor, no indication of leakage-current-induced failure.

This behaviour could be attributed to the relatively high doping levels and the superior dielectric insulation.

Figure 9 shows the characteristic curve of the poly-silicon sensor in the extended pressure range up to 5 times the operating pressure. All technological options showed sensitivities (dR/R) between 0.9 and 1.1 %.

The burst pressure of these sensors, loaded form the backside of the membrane, is higher than 8 times the nominal pressure. If the sensor is loaded from the front side, the burst pressure is even higher.

The characteristic curve deviation of the sensor can be seen in Fig. 10. Within the nominal pressure range all of the technological options showed a deviation smaller than 0.2 % full scale, the preferred option showed a deviation significantly less than 0.1 % fs.

When the sensor is overloaded, the compensation of the characteristic curve deviation works until ∼2.0 times the nominal pressure range where the maximum deviation is less than 0.06 % fs. Behind this extended range the deviation rises fast until 38 bar around 2.5 % fs is reached.

Because of the application field as a differential pressure sensor, the influence of an all-side static pressure was also tested.

The developed sensors that are 0-level packaged show a mean zero offset shift of 0.007 % fs at a static load of 100 bar (Fig. 11). This value is excellent, especially if it is compared to alternative packaging methods.

As explained earlier, one of the main goals was to develop a design that is insensitive to mounting stress. To evaluate this feature we deviated from the SFB as the packaging method and used anodic bonding. The anodically bonded packages were temperature loaded between 30 and 135 °C. For comparison purposes, this test was also performed with state-of-the-art sensors of different manufactures that are also focused on process measurement systems. These anodically bonded packages suffer from high strains at temperature changes as the thermal expansion of the used Borofloat glass is not perfectly matched to silicon. They also suffer from relaxation processes within the glass that lead to drift and hysteresis of the zero point offset at elevated temperatures (Blech et al., 2015).

The developed sensors outperform the state-of-the-art sensors in both tests (Figs. 12 and 13) and show their excellent stability against mounting stress. It should be much easier with these chips to transfer the excellent stability of the MEMS sensors to the measurement systems. This development approach should be taken more into consideration in the design phase as the best possible sensor is useless if its performance cannot be transferred to higher packaging levels.

The next tests should show the performance of the sensor at elevated temperatures. We decided to test the zero offset stability at different temperatures and times as well as the temperature dependency of the sensitivity. In the temperature range up to 300 °C, the dependency of the sensitivity adds up to −1.3 % fs per 100 K temperature increase.

The offset stability at 135 °C is < 0.003 % fs for 24 h and < 0.02 % fs for 2500 h. At 210 °C for 24 h an offset deviation of < 0.009 % fs could be achieved (Fig. 14) and even at 300 °C for 24 h the measurable drift was smaller than 0.03 % fs.

6 Summary and outlook

The developed SOI technology was shown to be suitable for the sensor production. The optimized SFB sensor packaging demonstrated its superior characteristics. The design goals for the sensor could be completely fulfilled. For the 300 °C temperature range an adjustment of the socket metallisation is needed as there are problems with the formation intermetallic phases (not shown here) at the contact areas.

Compared to similar sensor concepts (Sainan et al., 2015) the hysteresis, offset stability and non-linearity could be improved significantly. Compared to alternative sensor concepts like piezoresistive SiC pressure sensors, the developed sensor system cannot compete in terms of the maximum operating temperature range that is up to 750 °C with SiC sensors (Chung, 2010; Okojie et al., 2014). However, in terms of stability of the offset and temperature hysteresis the developed sensor is able to outperform these alternative concepts.

Acknowledgements. The authors acknowledge financial support by the Federal Ministry for Economic Affairs and Energy (BMWi, Grant No. MF110117).

Edited by: S. Zimmermann
Reviewed by: two anonymous referees

References

Blech, M., Übensee, H., Täschner, R., Brokmann, G., Xu, X., and Ortlepp, T.: Zeitkonstanten für die Relaxation thermomechanischer Spannungen in Silizium-Glas, 6th Mikrosystemtechnik-Kongress, 26–28 October 2015, Karlsruhe, Germany, 2015.

Bring, M.: Method for measuring fracture toughness of wafer-bonded interfaces with high spatial resolution, J. Micromech. Microeng., 16, S68–S74, 2006.

Burns, D. W.: "Micromechanical integrated sensors and the planar processed pressure transducer", PhD work, University of Wisconsin, Madison, WI, USA, 1988.

Celler, G. K. and Cristoloveanu, S.: Frontiers of silicon-on-insulator, J. Appl. Phys., 93, 4955–4978, 2003.

Chung, G. S.: Fabrication and Characterization of a Polycrystalline 3C-SiC Piezoresistive Micro-pressure Sensor, J. Korean Phys. Soc., 56, No. 6, 1759–1762, 2010.

Kanda, Y.: A Graphical Representation of the Piezoresistance Coefficient in Silicon, IEEE T. Electron. Dev., ED-29, No. 1, 1982.

Lechenault, F., Bouchaud, E., Rountree, C. L., Cousin, F., Bouchaud, J.-P., and Ponson, L.: Damage of silicate glasses during stress corrosion, J. Phys. Conf. Ser., 319, 012005, doi:10.1088/1742-6596/319/1/012005, 2011.

Okojie, R. S., Lukco, D., Nguyen, V., and Savrun, E.: Demonstration of SiC Pressure Sensors at 750 °C, Additional Conferences: January 2014, Vol. 2014, No. HITEC, 28–32, 2014.

Pawlik, M., Schechter, D., and Nicholas, K. H.: Resistivity and carrier concentration of doped c-Si, and sheet resistance of ion implanted bulk Si, Properties of crystaline silicon, London, UK, 1999.

Sainan, L., Ting, L., Wei, W., Yingping, H., Tingli, Z., and Jijun, X.: A novel SOI pressure sensor for high temperature application, Journal of Semiconductors, 36, No. 1, 014014, doi:10.1088/1674-4926/36/1/014014, 2015.

Soler, I. and Galo, J. A. A.: Molecular Chemistry of Sol-Gel Derived Nanomaterials, edited by: Corriu, R. J. P. and Anh, N. T., Angew. Chem. Int. Edit., 48, 8822–8823, doi:10.1002/anie.200904371, 2009.

Soßna E.: Herstellung von spannungsoptimierten Silizium-Membranen durch den elektrochemischen Ätzstopp an pn-Übergängen, Dissertation, Kassel, Germany, 2002.

Tufte, O. and Stelzer, E.: Piezoresistive properties of silicon diffused layers, J. Appl. Phys., 34, 313–318, 1963.

Wang, S. S., McNeil, V. M., and Schmidt, M. A.: An etch-stop utilizing selec-tive etching of N-Type silicon by pulsed potential anodization, J. Microelectromech. S., 1, 187–192, 1992.

Wohlgemuth, C.: Entwurf und galvanotechnische Fertigung metallischer Trennmembranen für mediengetrennte piezoresistive Drucksensoren, Dissertation, Darmstadt, Germany, 2008.

Yole Développement: MEMS report "Status of the MEMS Industry", 2015.